Supplemental Material

Supplemental Text

Bioreactor-derived 503FΔ*liaR* isolate with *divIVA*^{I92F} resisted DAP largely through an increased surface charge

DivIVA is a scaffold protein at the division septum and cellular poles that aids in septum formation and chromosomal segregation(1). In a previous study, *divIVA*^{Q75K} in *E. faecium* HOU503 was found to be correlated with DAP resistance through complex mechanisms that remain under study(2). When *divIVA*^{Q75K} was present, DAP resistance was mediated by a combination of modest increases in cell surface charge but we speculate that in light of recent work on the mechanism of action of DAP in *S. aureus*(3), mutations to DivIVA may mitigate mislocalization of this critical cell division protein induced by DAP effects on the cell membrane.

Here, *divIVA*^{I92F} was first observed on Day 5 and comprised 52% of the final 503FΔ*liaR* bioreactor population (**Figure 3a)** and found in two end-point isolates (**Table 3**). Both I92F and Q75K are in the predicted loop region between two N-terminal coiled coils, suggesting the importance of modifications in this region for DAP resistance. Using isolate 503FΔ*liaR* P25 (*divIVA*^{I92F}, *cls*^{R211L}, *entfae_126*^{V30*}), we found that this isolate produced abnormal division septa, bound less PLL:FITC (indicating a more positive surface charge) and some evidence of a subpopulation that hyperaccumulated DAP without redistributing anionic phospholipid microdomains (Figures S3, S1-S2). This was consistent with what was observed previously in the HOU503 *divIVA*^{Q75K} DAP-resistant isolates(2). The exact mechanism remains under investigation. Importantly, while we

observed a similar mutation that contributed to rapid acquisition of high levels of DAP resistance in HOU503(2), here, DAP adaptation in 503FΔ*liaR* was significantly delayed.

Bioreactor-derived 503FΔ*liaR* isolates with *murAA*^{A149E} may increase cell surface charge

MurAA catalyzes the first committed step in peptidoglycan synthesis by transferring enolpyruvate from phosphoenolphyruvate (PEP) to uridine diphospho-N-acetylglucosamine (UNAG). This reaction is targeted by the antibiotic fosfomycin (FOF), which irreversibly binds and inactivates the MurA active site(4, 5). The *murAA*^{A149E} allele was present at < 5% from Day 8-12 and grew to comprise 40% of the Day 18 population but then declined to 20% of the final population. *murAA*^{A149E} was present in 11/19 503FΔ*liaR* bioreactor-derived end-point isolates (Figure 2a and Table 3). A mutation within this enzyme could alter peptidoglycan synthesis leading to a remodeling of the cell wall, though there was no evidence of changes in cell wall thickness (Figure S5). It is possible that changes to the cell wall architecture may have decreased DAP access to the membrane, leading to increased resistance. These mutations, however, were observed in isolates with a variety of DAP MICs (ranging from 2-8 mg/L), suggesting that *murAA*^{A149E} alone was insufficient to confer resistance and additional mutations were required for high resistance levels.

Two *murAA*^{A149E} isolates with the fewest mutations, 503FΔ*liaR* P8 (*murAA*^{A149E}, *cls*^{A20D}, *entfae_809*^{A70E}, *entfae_64*^{Y83*}) and 503FΔ*liaR* P60 (*murAA*^{A149E}, *cls*^{N13I}, *entfae_126*^{V30*}), were selected for additional phenotypic analysis. Both isolates bound significantly less PLL:FITC than the ancestor without evidence of phospholipid microdomain remodeling (as visualized with NAO); however, paradoxically, both isolates

appear to bind more BDP:DAP than the ancestor (Figures S1-2,S4). So, while the cells had a modest increase in cell surface charge, it was not correlated with DAP repulsion. The presence of secondary mutations makes it difficult to make a clear association of *murAA*^{A149E} to DAP resistance. However, the consistent identification of *murAA*^{A149E} has led us to begin biochemical and structural studies of MurAA and MurAA^{A149E}. In general, isolates bound less PLL:FITC and did not redistribute lipid microdomains, suggesting that the changes in by MurAA^{A149E} function may indeed contribute to DAP-tolerance by changing the physical properties of the cell wall.

Interestingly, in 515FΔ*liaR, murAA*^{G220V} was observed in three bioreactor-derived end-point isolates, each of which had an additional 12-33 mutations (Table 4). An isolate containing this mutation (P53) also exhibited a minor increase in cell surface charge without evidence of DAP repulsion (Figure S6). Interestingly, this *murAA* mutation was located alongside nine additional mutations over 460 Kb that were identical to mutations acquired by a hypermutator subpopulation. It is possible that these mutations were part of a homologous recombination event. Further discussion can be found below.

VAN plasmid dynamics

503FΔ*liaR* is a vancomycin (VAN)-resistant isolate that contains a plasmid encoding *vanH, vanA, vanX, vanY,* and *vanZ.* This isolate has an initial VAN MIC of >256 mg/L. As was observed in HOU503 flask-transfer DAP adaptation (2), all flask-adapted strains of 503FΔ*liaR* resulted in VAN sensitivity with MICs falling from >256 to 2-8 µg/ml. 503FΔ*liaR* FT1-1/2, FT2-1/2, FT3-1, and FT4-1/2 all lost the VAN plasmid, as was observed in HOU503 adaptation (2). 503FΔ*liaR* FT5-1/2, however, showed evidence of reduced VAN coverage in the pileups, suggesting a reduction in plasmid copy number

which may contribute to the increase in VAN sensitivity. Because FT5-1/2 contained a *yvcS* mutation and had VAN plasmid coverage, this suggests that mutations to *yvcRS* do not necessitate the removal of the VAN plasmid. Instead, because flask-transfer isolates with multiple genotypes do lose the VAN plasmid, it suggests that the flask environment selects against VAN plasmid maintenance.

Renewed VAN sensitivity was also observed in several 503FΔ*liaR* bioreactor-derived isolates with diverse mutational profiles. There was no evidence of total plasmid loss in these isolates, however (Table S1). The VAN plasmid contains multiple transposases and insertional elements that are present in multiple locations throughout the *E. faecium* genome, causing these regions to spike in coverage when analyzing the read data. The unique regions on the plasmid include *vanHAX*. To determine if plasmid copy number was being affected, the ratio of average unique read coverage on the VAN plasmid compared to the average coverage of that isolate's genome was examined. Using this metric, there was no correlation between the plasmid coverage and the VAN MIC (Table S1). Therefore, it is likely that an undefined mechanism contributes to this increase in VAN sensitivity observed in diverse backgrounds and we are observing the "see-saw" effect.

515FΔ*liaR* evolution in a bioreactor

515FΔ*liaR* mutations that were present at a minimum of 10% frequency for two consecutive days can be found in Figure 2b. Interestingly, four different genes contained mutations on Day 1. Five separate mutations were found downstream of the Plasmid 169-encoded *repA* on Day 1 comprising a total of 53% of the starting population. These SNPs were located +450, +496, +501, +558, and +718 nucleotides downstream of *repA* and

manual visualization of the sequencing reads suggests that these mutations were exclusive of each other. However, these mutations were not present in a no DAP bioreactor experiment, suggesting their importance in aiding against DAP. *Entf515F_2210, entf515F_641,* and *entf515F_3080,* also present on Day 1, dropped in frequency upon DAP addition; each mutation was then able to find some success throughout adaptation but did not reach high frequencies- consistent with hitch-hiking. Interestingly, *murAA*^{G220V} was first observed on Day 6 and maintained a low-level presence within the bioreactor throughout the rest of adaptation. This suggests that while *murAA*^{G220V} had success in this population, other mutations provided a more significant advantage. The *metB*$^{+C}$ mutation appeared on Day 9 while *metB*$^{+T}$ and *rpoA*^{N288K} first made an appearance on Day 10. These two populations then competed against each other in the bioreactor as evidenced by their opposing frequency profiles. Towards the end of adaptation, additional mutations likely contributed modest advantages in the DAP environment. Interestingly, **NO** mutations were observed in *cls*.

Perhaps surprisingly, a bioreactor-derived subpopulation developed a hypermutator phenotype by gaining a mutation in mismatch repair (MMR) gene, *mutM.* This mutation likely resulted in improper MMR causing the indiscriminate accumulation of a variety of mutations. Here, 515FΔ*liaR* P86 acquired 42 mutations (Table 3). This strategy of rapidly accumulating mutations in response to antibiotic stress has been observed in a variety of bacteria, including *Acinetobacter baumannii* and *Pseudomonas aeruginosa* (6, 7)*. mutM*^{L14F} first appeared at 5% on Day 15 but never reached over 10% of the population, and thus, is not represented in Figure 3b. Of note, this population acquired nine mutations over 460 Kb of the genome, including *murAA*^{G220V} and *liaY*^{Y74N}*,*

that were identical in 515FΔ*liaR* P31 and P53. Because the frequency of these mutations was not readily apparent before Day 10, when *metB*$^{+T}$ first appeared, it is possible that homologous recombination occurred from P86 into the P31/P53 lineage.

515FΔ*liaR* no-DAP adaptation

Because the *metB* mutations marked that a likely global change in metabolism was used to combat DAP, we wanted to confirm that these mutations evolved in response to DAP and not to the bioreactor environment itself. Therefore, 515FΔ*liaR* was evolved in the bioreactor with no DAP present for 12 days, when *metB* mutations had comprised a combined 68% of the population in the presence of DAP. At the end of this experiment, the final day population was sent for metagenomic sequencing. No mutations were present within *metB,* consistent with these mutations evolving in response to DAP and not the bioreactor environment. Mutations downstream of *repA* were not observed either, suggesting their supportive role in DAP resistance.

***metB* fusion protein**

Surprisingly, in HOU503 and *E. faecium* DO, this gene fusion is already present, and align with 99% identity to the fusion found in DAP resistant 515FΔ*liaR* (Figure S8). The ability to switch from two gene products to one based upon a single base pair insertion suggests that this genome has recently diverged from HOU503 and DO. In HOU503, this full-length gene is annotated as *metB,* while in DO, it is annotated as *metC,* which in *E. coli* encodes cystothionase (8). The high levels of homology between *met* genes makes it difficult to assert identity and protein function (9). The 515FΔ*liaR* fusion protein aligns with 42% identity to *E. coli* K12 MetB and 31% identity to MetC, suggesting

that the fusion (or single protein in the case of HOU503 and DO) has similar activity to MetB. Extensive biochemical analyses need to be performed to verify the role this gene plays in cysteine metabolism in enterococci.

515FΔ*liaR* punctate NAO phenotype

When incubated with NAO, 515FΔ*liaR* P29 (*metB*$^{+C}$, sortase insertion, *gdpD*^{H29R}, *entf515f*_1865^{A327E}) and P51 (*metB*$^{+T}$, *rpoA*$^{+500}$, r*epA*$^{+718}$, *yvcR*^{G15S}, *entf515F*_191^{V336V}) produced a “dotted” phenotype, where NAO binding condensed to a single focal point in cells (Figures S7). Surprisingly, this redistribution of phospholipids does not show evidence of redistributed DAP binding. This was the first instance where we observe phospholipid redistribution without DAP redistribution. This phenotype was not observed in other isolates containing either *metB* mutation and the lack of similar alleles between these two isolates suggests that this dot phenotype is the result of convergent evolution.

Plasmid-encoded mutations

Mutations downstream of a plasmid-encoded *repA* are found in HOU503(2), 503FΔ*liaR,* and 515FΔ*liaR* adaptation (Tables 2-4). How exactly these mutations contribute to DAP resistance remains unclear. Interestingly, in 515FΔ*liaR* adaptation, when *repA* mutations were not present, the insertion of an insertional sequence element into *entf515F_3139* (a Type A Sortase) appeared- this gene is located on the same plasmid. When isolates with this insertion underwent RNAseq analysis, it was determined that the two downstream genes, *entf515F_3140-3041* (encoding an O-antigen like family protein and type A sortase, respectively) had increased expression compared to the ancestor, suggesting that these two genes may play a role in DAP resistance (data not shown). Type A Sortases pay a role in gut colonization (10) and it is possible that these

mutations aided in adhesion within the bioreactor environment. Of note, mutations within sortases were not observed in flask-transfer populations. HOU503 Plasmid 1 and 515FΔ*liaR* Plasmid 169 have homology between their sequences that encompasses 33 genes and includes *repA* and *entf515F_3041-3042.* Further qPCR should be performed in HOU503, 503FΔ*liaR,* and 515FΔ*liaR* to determine if all end-point isolates containing *repA* mutations have increased *entf515F_3041* expression.

Supplemental References

1. Pinho MG, Errington J. 2004. A divIVA null mutant of Staphylococcus aureus undergoes normal cell division. FEMS Microbiol Lett 240:145–149.

2. Prater AG, Mehta HH, Kosgei AJ, Miller WR, Tran TT, Cesar A, Shamoo Y. 2019. Environment shapes the accessible daptomycin resistance mechanisms in Enterococcus faecium. Antimicrob Agents Chemother.

3. Grein F, Müller A, Scherer KM, Liu X, Ludwig KC, Klöckner A, Strach M, Sahl HG, Kubitscheck U, Schneider T. 2020. Ca2+-Daptomycin targets cell wall biosynthesis by forming a tripartite complex with undecaprenyl-coupled intermediates and membrane lipids. Nat Commun 11:1–11.

4. Kahan FM, Kahan JS, Cassidy PJ, Kropp H. 1974. The mechanism of action of fosfomycin (phosphonomycin). Ann N Y Acad Sci 235:364–386.

5. Skarzynski T, Mistry A, Wonacott A, Hutchinson SE, Kelly VA, Duncan K. 1996. Structure of UDP-N-acetylglucosamine enolpyruvyl transferase, an enzyme

essential for the synthesis of bacterial peptidoglycan, complexed with substrate UDP-N-acetylglucosamine and the drug fosfomycin. Structure 4:1465–1474.

6. Hammerstrom TG, Beabout K, Clements TP, Saxer G, Shamoo Y. 2015. Acinetobacter baumannii repeatedly evolves a hypermutator phenotype in response to tigecycline that effectively surveys evolutionary trajectories to resistance. PLoS One 10:e0140489.

7. Mehta HH, Prater AG, Shamoo Y. 2017. Using experimental evolution to identify druggable targets that could inhibit the evolution of antimicrobial resistance. J Antibiot (Tokyo) 1–8.

8. Simon M, Hong JS. 1983. Direct homocysteine biosynthesis from O-succinylhomoserine in Escherichia coli: An alternate pathway that bypasses cystathionine. J Bacteriol 153:558–561.

9. Ferla MP, Patrick WM. 2014. Bacterial methionine biosynthesis. Microbiol (United Kingdom) 160:1571–1584.

10. Kristich CJ, Chandler JR, Dunny GM. 2007. Development of a host-genotype-independent counterselectable marker and a high-frequency conjugative delivery system and their use in genetic analysis of Enterococcus faecalis. Plasmid 57:131–144.

Supplemental Figures

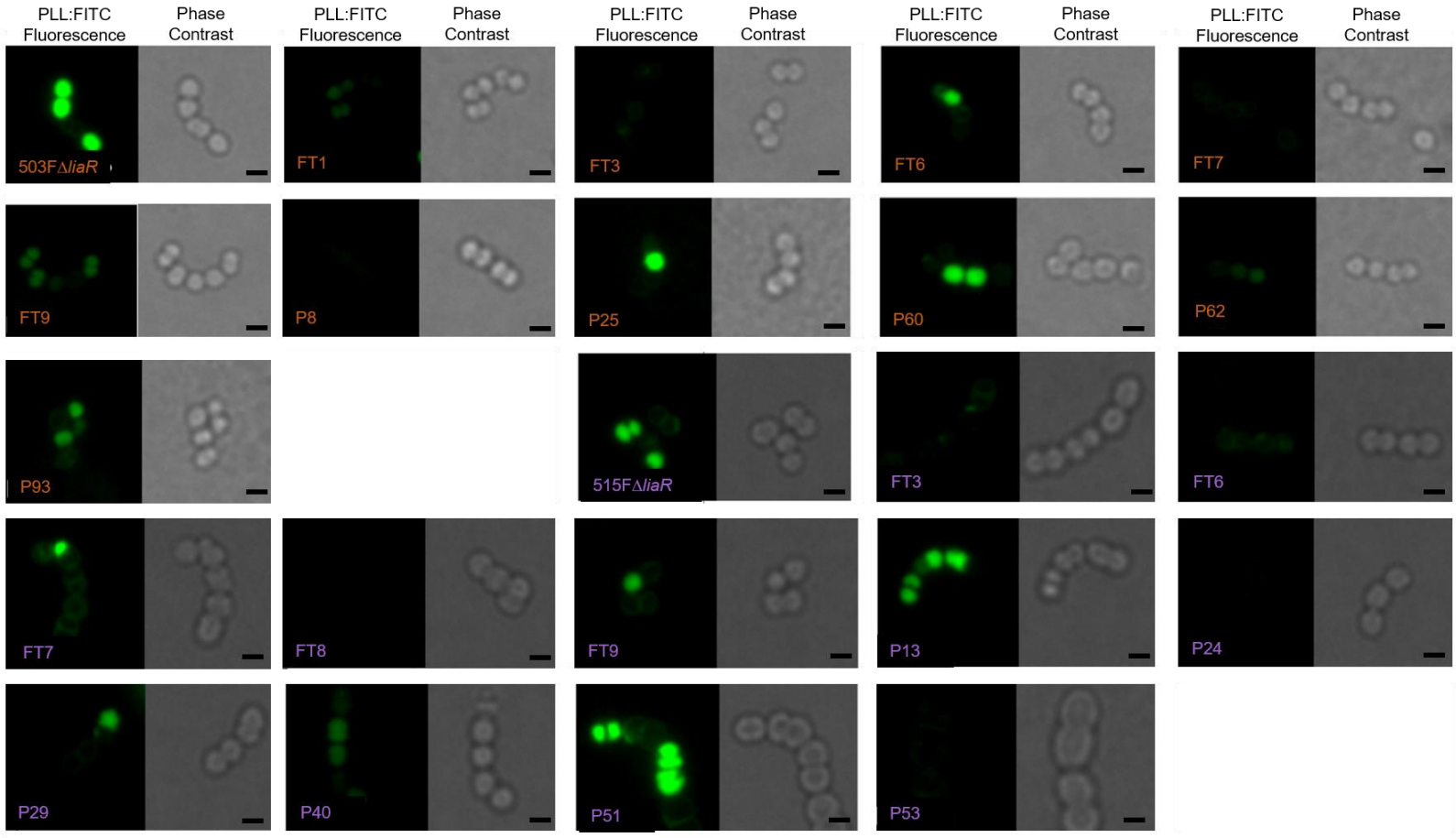
PLL:FITC Fluorescence
Phase Contrast
503FΔliaR
FT1
FT3
FT6
FT7
FT9
P8
P25
P60
P62
P93
515FΔliaR
FT3
FT6
FT7
FT8
FT9
P13
P24
P29
P40
P51
P53

Figure S1. **DAP-resistant end-point isolate PLL:FITC binding patterns**. Isolates were incubated with PLL:FITC to determine cell surface charge. Isolates in orange were derived from 503FΔliaR while isolates in purple were derived from 515FΔliaR. Scale bars show 1 µm**.**

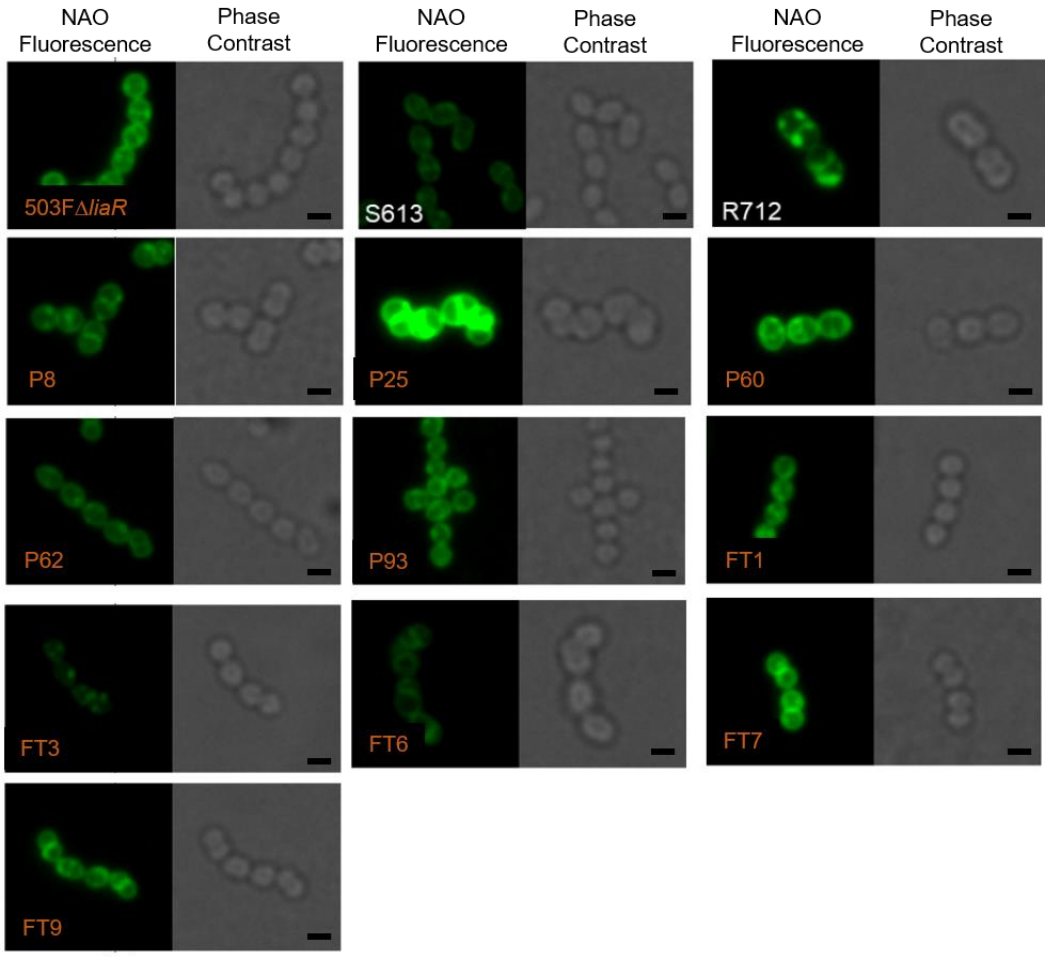

Figure S2. 503FΔ*liaR* isolates incubated with NAO. Isolates were incubated with NAO to determine membrane phospholipid distribution. *E. faecalis* S613 is a control showing uniform NAO staining while *E. faecalis* R712 is a control showing phospholipid redistribution. Scale bars indicate 1 µm.

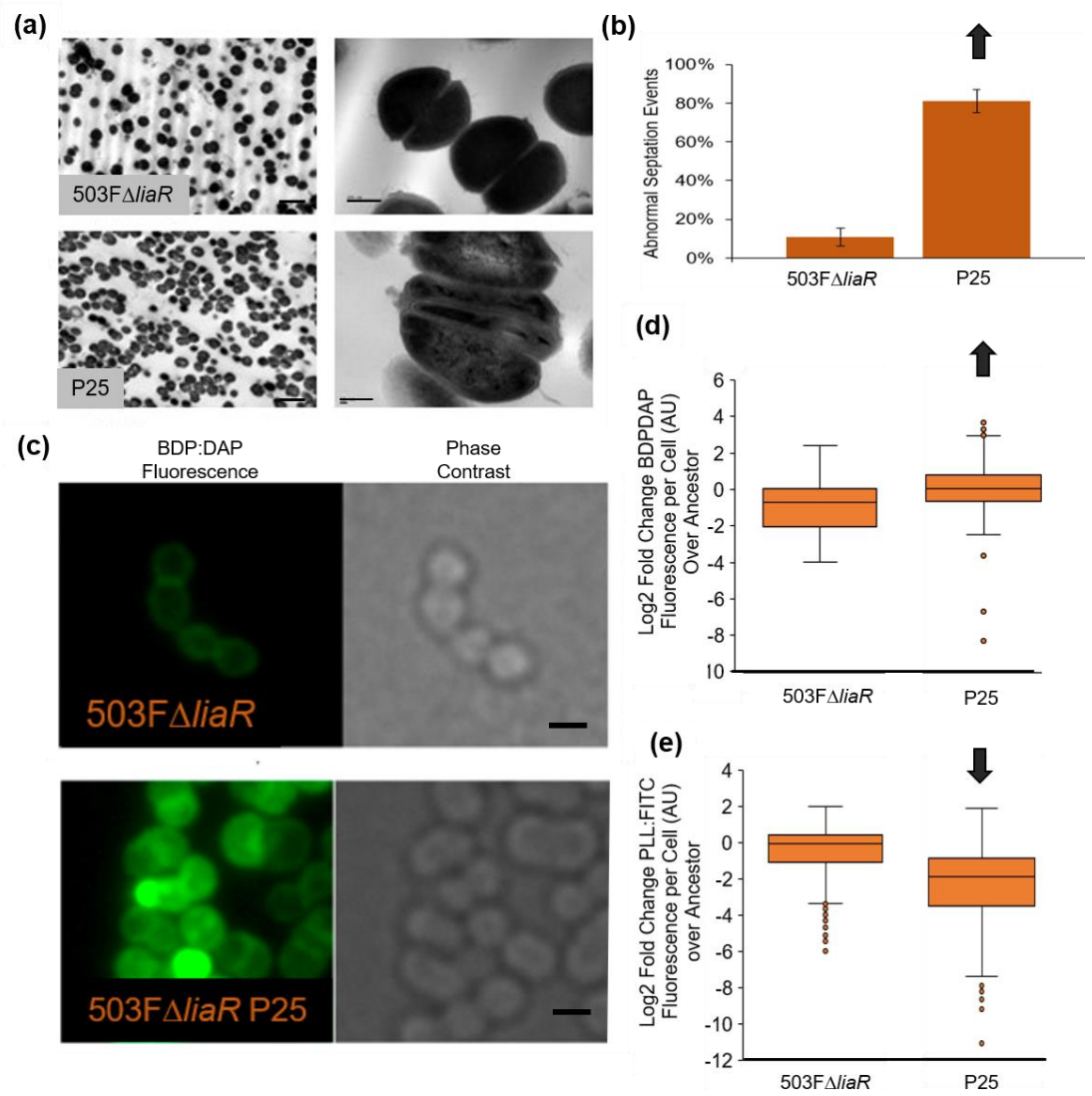

Figure S3. 503FΔ*liaR* bioreactor-derived isolate with *divIVA*^{I92F} had aberrant septal formation. **(a)** TEM with scale bars indicating 2 µm (left) and 200 nm (right). **(b)** Aberrant septation events were quantified and significance determined by Student's T test with ($p<0.05$). **(c)** Isolates incubated with 32 µg/ml BDP:DAP with scale bars indicating 1 µm. **(d)** Quantification of BDP:DAP using ImageJ. **E.** Quantification of PLL:FITC using ImageJ. Images found in **Figure S1.** Arrows indicate significance compared to the ancestor ($p<0.05$) using Mann-Whitney with *post hoc* Holm-Bonferroni adjustment. Experiment performed in duplicate on separate days.

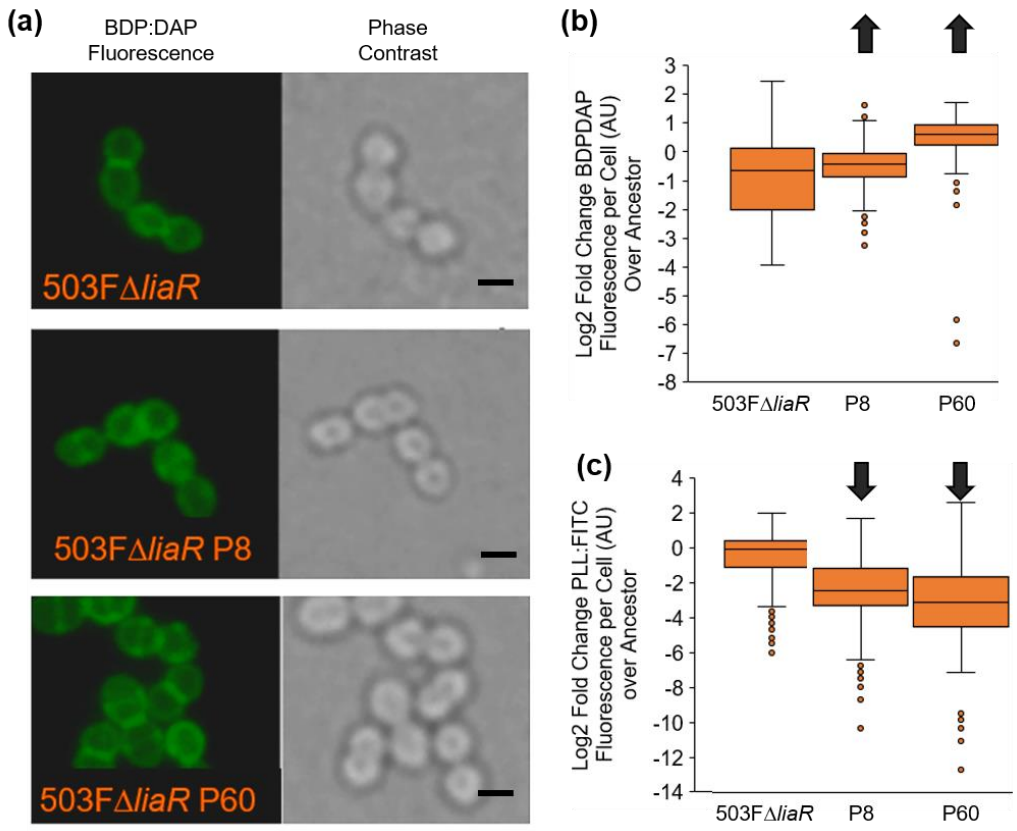

220

221 **Figure S4. 503FΔ*liaR* bioreactor-derived isolates with *murAA*^{A149E} may increase cell**
222 **surface charge.** **(a)** Isolates incubated with 32 µg/ml BDP:DAP. Scale bars indicate 1
223 µm. **(b)** Quantification of BDP:DAP using ImageJ. **(c)** Quantification of PLL:FITC using
224 ImageJ. Images found in **Figure S1.** Arrows indicate significance compared to the
225 ancestor ($p<0.05$) using Mann-Whitney with post hoc Holm-Bonferroni adjustment.
226 Experiment performed in duplicate on separate days.

227

228

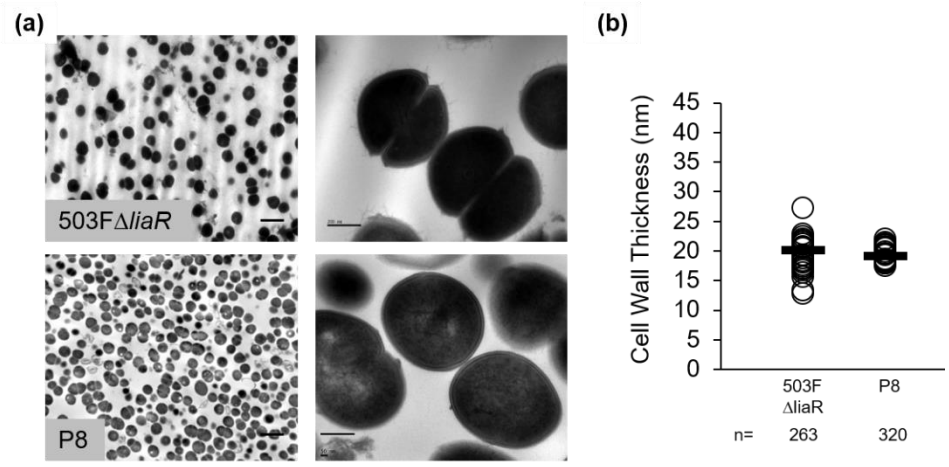

229

230 **Figure S5. 503FΔ*liaR* bioreactor-derived isolate with mutation to *murAA* does not**
231 **have altered cell morphology. (a)** TEM to observe cell morphology of 503FΔ*liaR* (top)
232 and P8 (*murAA*^{A149E}, *cls*^{A20D}, *entfae_809*^{A70E}, and *entfae_64*^{Y83*}; bottom) with scale bars
233 showing 2 µm (left) and 200 nm (right). **(b)** ImageJ was used to quantify cell wall thickness
234 in each isolate. No statistical significance ($p<0.05$) was observed using Student's T-Test.

235

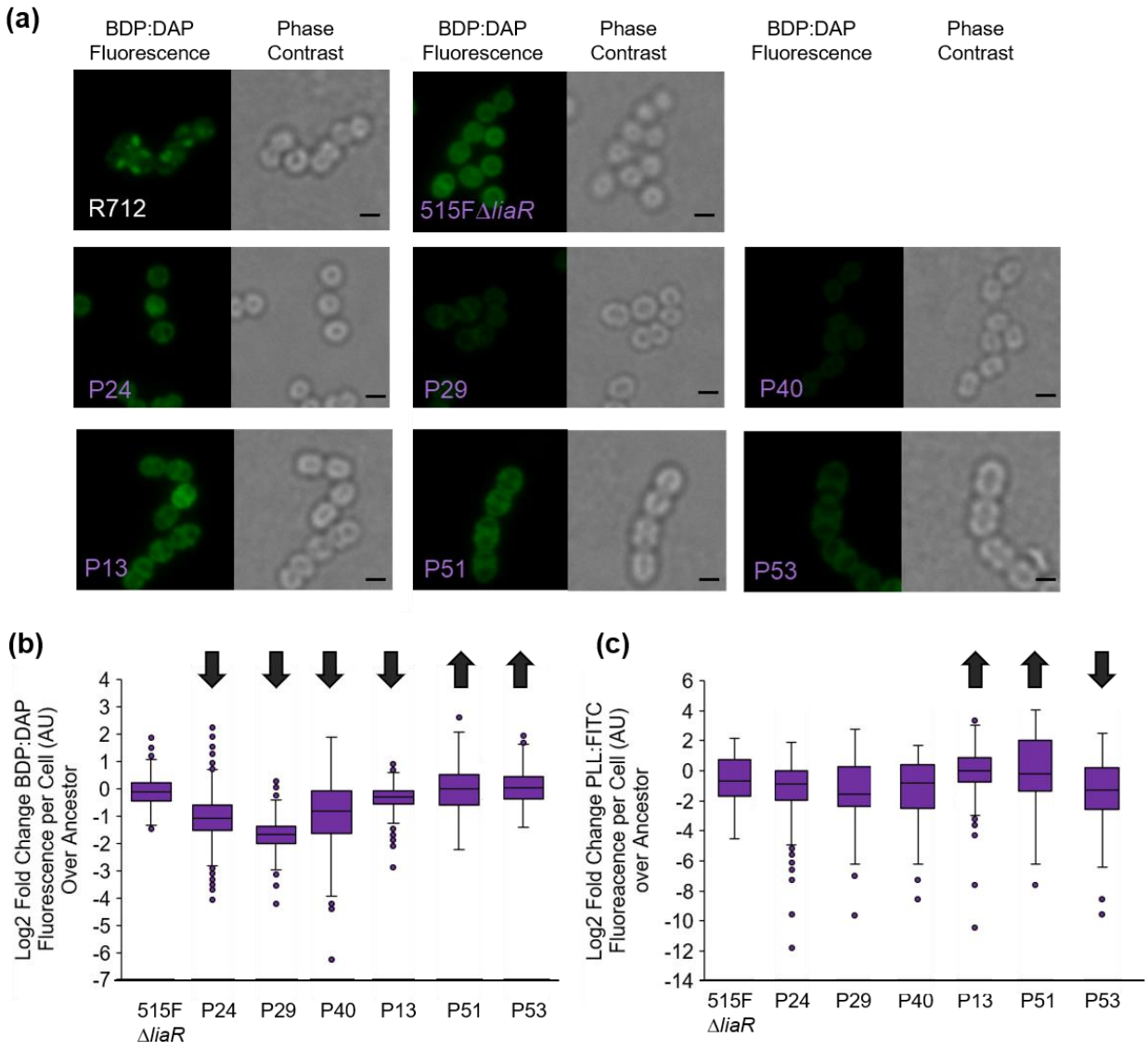

Figure S6. 515FΔ*liaR* bioreactor-derived isolates with *metB* mutations produced variable phenotypes. (a) Isolates incubated with 32 µg/ml BDP:DAP. *E. faecalis* R712 is a control showing redistributed BDP:DAP binding. Scale bars indicate 1 µm. **(b)** Quantification of BDP:DAP using ImageJ. **(c)** Quantification of PLL:FITC using ImageJ. Images found in **Figure S1.** Arrows indicate significance compared to the ancestor ($p<0.05$) using Mann-Whitney with post hoc Holm-Bonferroni adjustment. Experiment performed in duplicate on separate days.

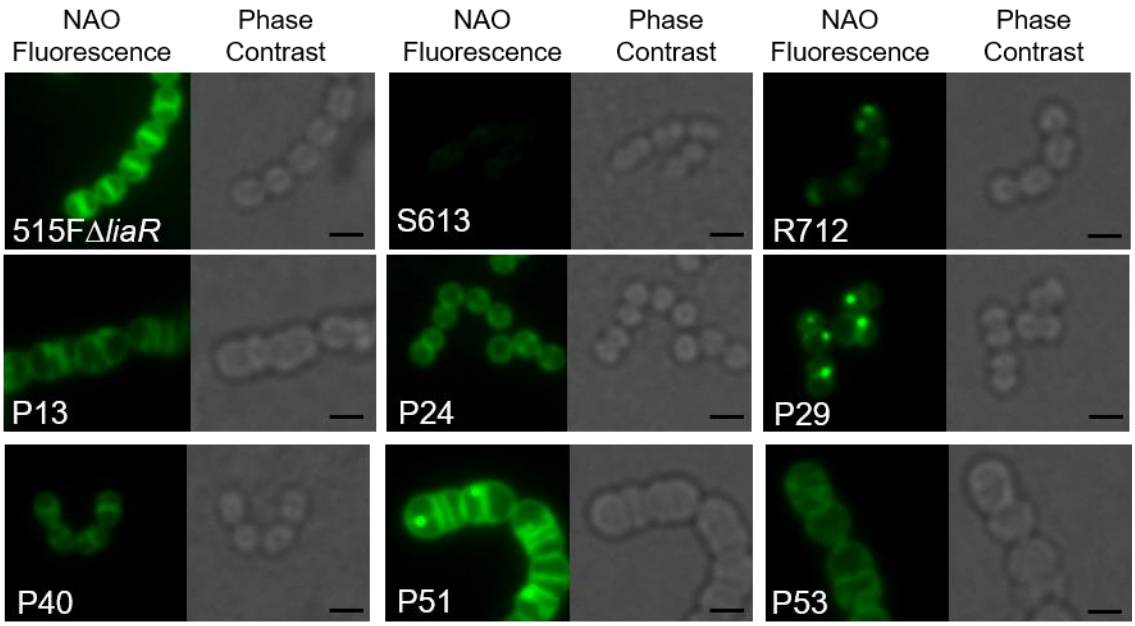

244

245 **Figure S7. 515FΔ*liaR* bioreactor-derived isolates with *metB* mutations produce**
246 **interesting membrane structures.** Isolates were incubated with NAO to identify
247 differences in membrane structure.

248

249

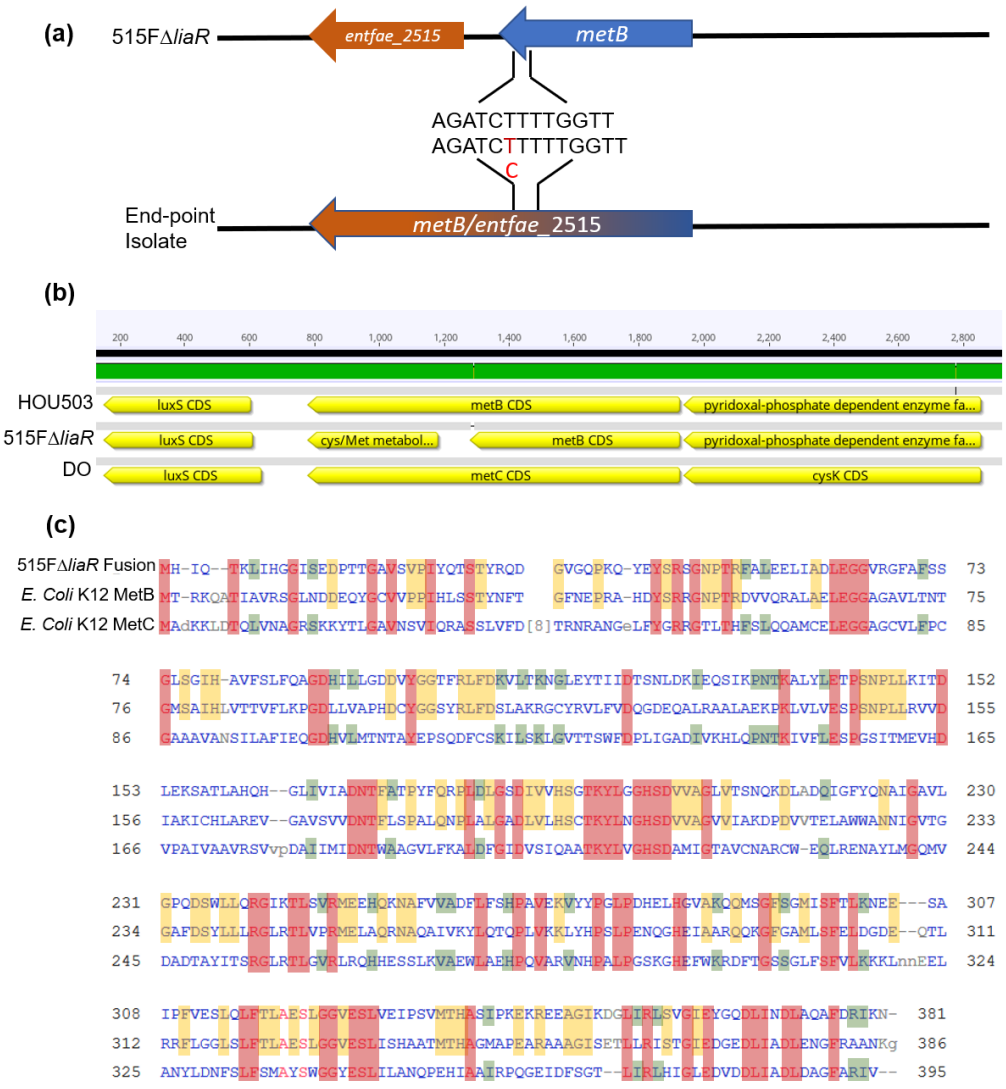

Figure S8. 515FΔ*liaR metB* mutations resulted in the in-frame fusion of two gene products. **(a)** Schematic representation of the nucleotide insertion site. **(b)** Alignment of three E. faecium genomes showing the relatedness of these species. **(c)** Alignment of 515FΔliaR fusion protein with E. coli MetB and MetC showing identities- red is shared by all, yellow with MetB, and green with MetC.

Supplementary Tables

Table S1. 503FΔ*liaR* bioreactor-derived isolate VAN plasmid coverage.

	Genome Avg Cov	Plasmid Avg Cov	Plasmid:Genome Ratio	VAN MIC
503FΔliaR	353	338	0.96	>256
P8	328	117	0.36	>256
P15	385	460	1.19	2
P25	456	216	0.47	2
P30	413	333	0.81	2
P33	491	200	0.41	2
P40	444	143	0.32	>256
P49	402	141	0.35	>256
P50	423	133	0.31	256
P55	456	289	0.63	2
P56	413	588	1.42	2
P57	448	1000	2.23	2
P59	377	227	0.60	2
P60	422	316	0.75	2
P62	416	240	0.58	2
P65	406	958	2.36	2
P69	382	706	1.85	2
P70	365	211	0.58	2
P79	387	185	0.48	>256
P83	468	356	0.76	2
P93	402	399	0.99	2